SPICE Electrical Models and Simulations of Silicon Photomultipliers

Federica Villa, *Member, IEEE*, Yu Zou, Alberto Dalla Mora, Alberto Tosi, *Member, IEEE*, and Franco Zappa, *Senior Member, IEEE*

Abstract—We present and discuss a comprehensive electrical model for Silicon Photomultipliers (SiPMs) based on a microcell able to accurately simulate the avalanche current build-up and the self-quenching of its Single-Photon Avalanche Diode (SPAD) "pixel" with series-connected quenching resistor. The entire SiPM is modeled either as an array of microcells, each one individually triggered by independent incoming photons, or as two macrocells, one with microcells all firing concurrently while the other one with all quiescent microcells; the most suitable approach depends on the light excitation conditions and on the dimension (i.e. number of microcells) of the overall SiPM. We validated both models by studying the behavior of SiPMs in different operating conditions, in order to study the effect of photons pile-up, the deterministic and statistical mismatches between microcells, the impact of the number of firing microcells *vs*. the total one, and the role of different microcell parameters on the overall SiPM performance. The electrical models were developed in SPICE and can simulate both custom-process and CMOS-compatible SiPMs, with either vertical or horizontal current-flow. The proposed simulation tools can benefit both SiPM users, e.g. for designing the best readout electronics, and SiPM designers, for assessing the impact of each parameter on the overall detection performance and electrical behavior.

Index Terms—Electrical model, electrical simulation, photoelectron spectrum, photon pile-up, silicon-photomultiplier (SiPM), single-photon avalanche diode (SPAD), SPICE modelling, transient analysis.

I. INTRODUCTION

SINGLE-PHOTON detectors find widespread use in nuclear research and in biological and medical imaging. Photomultiplier Tubes (PMTs) have been employed for their single-photon sensitivity, photon-number-resolving capability and large active area. Single-Photon Avalanche Diodes (SPADs) [1] are often preferred to photomultipliers, because they are solid-state, rugged and require single lower power supply.

F. Villa, A. Tosi, and F. Zappa are with the Dipartimento di Elettronica, Informazione e Bioingegneria of Politecnico di Milano, I-20133 Milano, Italy, and also with the Istituto Nazionale di Fisica Nucleare (INFN) - Sezione di Milano, I-20133 Milano, Italy (e-mail: federica.villa@polimi.it; alberto.tosi@polimi.it; franco.zappa@polimi.it).

Y. Zou is with the Dipartimento di Elettronica, Informazione e Bioingegneria of Politecnico di Milano, I-20133 Milano, Italy (e-mail: yu.zou@polimi.it).

A. Dalla Mora is with the Dipartimento di Fisica of Politecnico di Milano, I-20133 Milano, Italy (e-mail: alberto.dallamora@polimi.it).
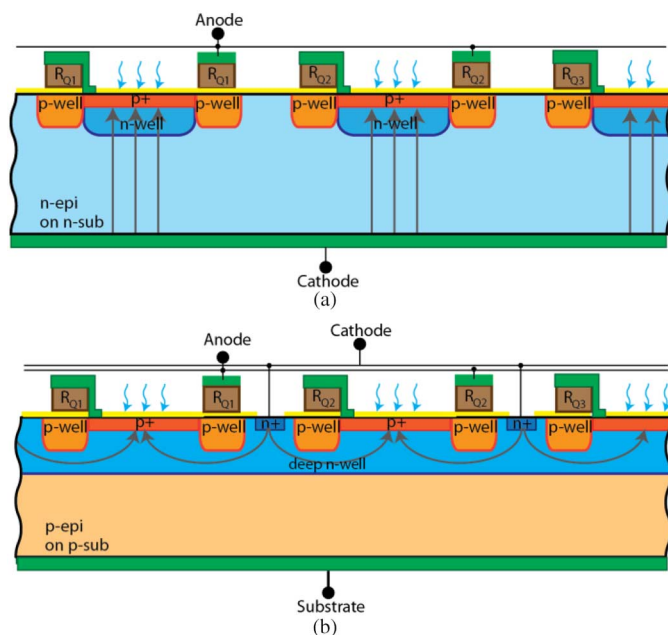

Fig. 1. Example of SiPM cross-sections with vertical (a) and horizontal (b) current-flow, shown as gray arrows. Note the quenching resistor R_Q added in series to each SPAD junction.

Silicon-Photomultipliers (SiPMs) offer both single-photon sensitivity, photon-number-resolving capability, and large active area all within a solid-state and rugged device [2].

An analog SiPM is a device composed by many (hundreds or thousands) parallel-connected microcells, each one consisting of a SPAD in series to a quenching resistor. Digital SiPMs instead are more complex devices [3], with an integrated active quenching circuit into each microcell and some other digital circuitry, like switches, latches or even Time-to-Digital Converters. Many commercially-available analog SiPMs are developed in custom technologies and usually have vertical current-flow structures, with a top anode and a backside cathode (or vice versa) electrodes [4]–[11]. Analog SiPMs have been developed also in standard CMOS technologies, with a horizontal current-flow structure [12], usually through a well or epi-layer, and present two topside electrodes (anode and cathode) and a third backside substrate electrode. The two different structures, shown in Fig. 1, mainly impact on photo-detection efficiency (PDE), but also on parasitic capacitances and electrical transient behavior, due to such a third electrode. In this paper we present a comprehensive SPICE electrical model [13] for SiPMs, which overcomes the limitations of other SiPM models so far reported or adds additional features. For example, some works [14],
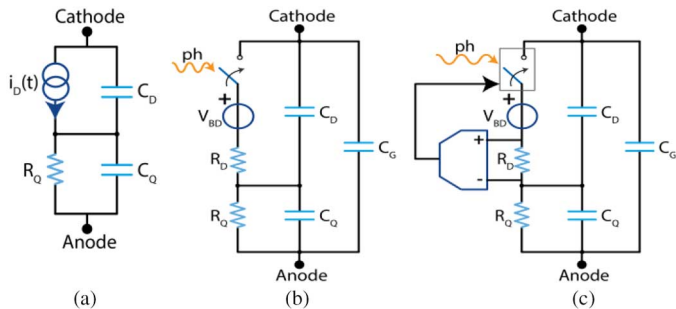
Fig. 2. Different SiPM microcell models reported in literature: (a) as a current generator [14], [15], (b) as switch and voltage generator with fixed avalanche duration [16], [19], (c) as a self-quenching microcell [17], [18].

Fig. 3. Proposed SiPM microcell schematics (left) and symbol (right).

[15] model each SiPM microcell as a current generator, which injects a current pulse, with constant amplitude and duration, into the load (see Fig. 2(a)). Instead in real SiPMs, current amplitude and duration depend on quenching resistor, parasitic capacitances, and excess bias applied to the device above its breakdown voltage.

In an improved model [16], a switch mimics the ignition of the avalanche while a voltage generator sets the breakdown voltage (see Fig. 2(b)); in that way the current amplitude is free to vary, but the duration is still fixed and set by the switch closure duration. Instead, the self-quenching time depends on the quenching resistor and, if too low, the avalanche current could even not get quenched. Furthermore, that model [16] presents only one decay time constant, without considering the second slower decay, which intervenes when the switch gets open. In [16] an entire SiPM with N microcells was modeled as two components, one representing F simultaneously fired microcells (i.e. all hit by concurrent photons) while the remaining N–F microcells were still quiescent. An analytical discussion of the avalanche current transient dependence on total and fired microcells was presented, but with no validating simulation. A limitation of that model was that only simultaneous avalanches (i.e. photon bunches) could be modeled. Another paper [17] proposed how to implement the self-quenching within the model (see Fig. 2(c)), but neither simulations nor computations or validations were presented. Another accurate model is proposed and validated in [18]: it correctly simulates self-sustaining and self-quenching avalanches of single and multiple microcells. However that model can be applied only to vertical current-flow devices (with two terminals) and emulates only simultaneous photon ignitions.

Ref. [19] reported a microcell very similar to [16], but the overall SiPM was modeled as the parallel connection of N microcells; in that way avalanches triggered by photons arriving not simultaneously and parasitic resistances among microcells could be analyzed, but just for small (e.g. 4×4) arrays.

The SiPM model presented in this paper stems from the SPICE model for SPAD detectors we presented in [20], which included avalanche self-quenching when the current got lower than a set threshold. Here we enrich that model to be suitable for SiPMs with many more parasitic components and couplings. Moreover, we propose to simulate the entire SiPM as either two macrocells (one for all firing microcells and the other one
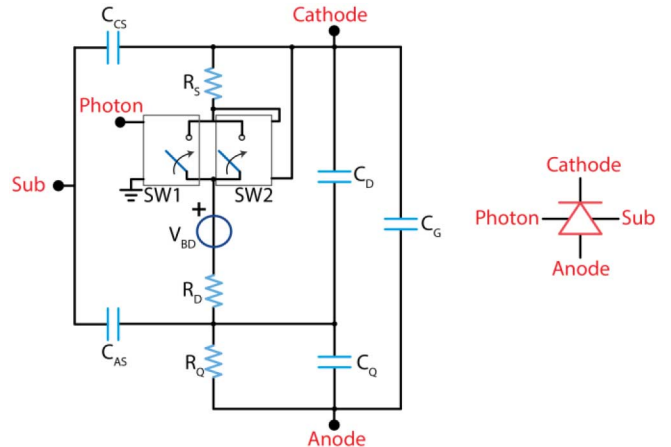
for not-firing ones), like in [16] and [18], or an array of individually-triggerable parallel-connected independent microcells, like in [19], for a much more refined simulation of all parasitic effects from layout to schematics (i.e. during post-layout analysis). Furthermore, while models reported so far can simulate only vertical current-flow SiPMs, our models include also the substrate contact (a third pin, apart from "Photon" excitation),excitation), which is responsible for added parasitics and major waveform differences in the readout from either anode or cathode in horizontal current-flow SiPMs. Such differences can be estimated with none of the models proposed so far. The microcell modelling and the two simulation approaches can be both employed by SiPM users, in order to select the best readout circuitry for each application, and by SiPM device designers, in order to study the effect of different SPAD shapes and sizes, quenching resistances, interconnects, and parasitic effects.

II. SiPM Microcell Model

Fig. 3 shows the SiPM microcell model and symbol, in which breakdown voltage V_{BD}, intrinsic (junction space-charge) SPAD resistance R_D, quenching resistance R_Q, and stray capacitances are user-adjustable parameters. The detector capacitance C_D is the SPAD junction capacitance, instead the anode-to-substrate C_{AS} and the cathode-to-substrate C_{CS} stray capacitors are present only in horizontal current-flow SiPMs and they can be set to a few acto-Farad (almost zero) when modeling vertical current-flow SiPMs, where the substrate node has to be left floating (since not present). It is important to note that in some SiPMs the quenching capacitance C_Q is just a stray unwelcome parasitic component, whereas in others it is increased on purpose, in order to improve the SiPM timing performance, i.e. the fast peaked response [21]. Eventually, the distributed grid capacitance C_G is due to the metal grid for the (parallel microcells) interconnects.

As shown in Fig. 3, the *Photon* pin is used to ignite the avalanche (by means of a 500 mV squared pulse with 200 ps duration), by closing the voltage-controlled switch SW1. R_S is a small-value (0.1 Ω) resistor used by current-controlled switch SW2 to monitor the microcell current: when the avalanche current exceeds a set (we used 60 μA) threshold the switch
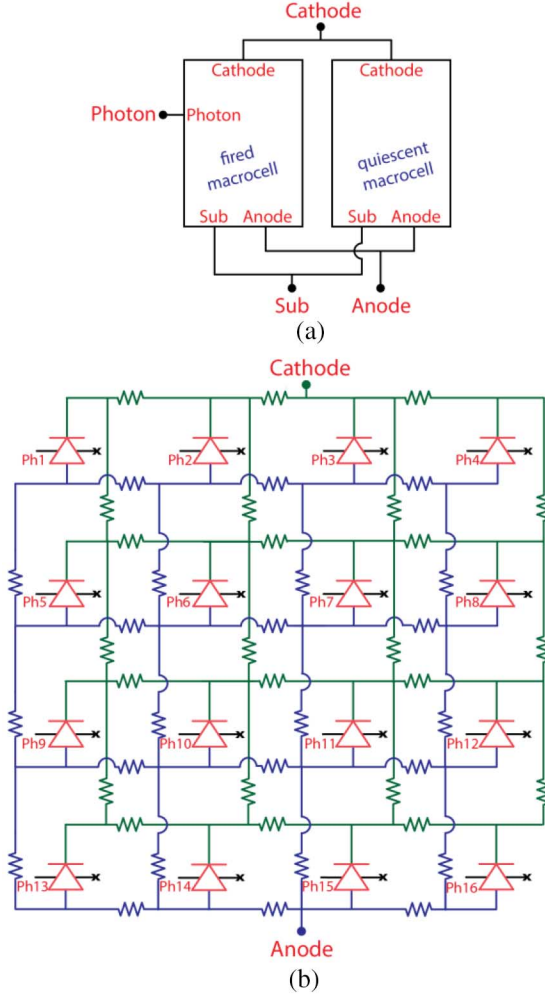
(a)

(b)

Fig. 4. Entire SiPM modelled as either (a) two macrocells, one for the simultaneously-fired microcells and the other one for those remaining quiescent, or (b) as an array of individually triggered microcells.

SW2 closes (avalanche self-sustaining process) whereas it opens when the avalanche current becomes lower than a second threshold (avalanche self-quenching), that we set at 50 μA, in order to introduce a small hysteresis.

As a first order approximation, the avalanche breakdown knee can be modelled as a constant value V_{BD}. However, in case of avalanche current crowding effects or non-linear current-voltage curve, a piecewise linear modelling can be easily implemented as shown in [20].

III. MACROCELLS AND ARRAY SIMULATION APPROACHES

For modelling the entire SiPM, we conceived two different approaches, depicted in Fig. 4, depending on the photonic excitation of interest and on the type of simulation to implement. In the *two macrocells approach*, the SiPM is modelled as two macrocells, one representing F fired microcells (out of the total N ones), while the other one representing the remaining (N–F) not-firing quiescent microcells, as shown in Fig. 4(a). Each macrocell is simulated as just one circuit shown in Fig. 3, in which the quiescent macrocell has the *Photon* excitation input disabled. Since in SiPMs all microcells are connected in parallel, within the firing macrocell model the resistance

values are equal to those of a single microcell divided by F, while capacitances are multiplied by F. In the same way, the quiescent macrocell model has resistances divided by N–F and capacitances multiplied by N–F. The *two macrocells* approach is suitable when SiPM with a very large number of microcells must be modelled for simulating "intense" (multiple and coincident) photon excitations or when a coarse and fast simulation suffices, with no need to distinguish (either in time t or in space x-y domain) among which microcell was fired. Furthermore, three or more macrocells can be employed to simulate photon bunches excitations hitting the SiPM in two or more time-instants.

Instead, when it is important to simulate the effect of non-coincident photons over the whole SiPM, or when either statistical or deterministic mismatches among microcells must be investigated, or when parasitic effects of the arrayed interconnects come into play, the second approach is to be preferred, where the SiPM is actually simulated as an array of X by Y microcells, each one individually triggered through the corresponding *Photon* excitation pin. Fig. 4(b) shows this *array approach*, where anode and cathode interconnects are shown with their parasitic resistance among microcells, whereas parasitic capacitance and substrate network are not shown for the sake of clarity. We used this approach also to add tolerances to the values of V_{BD}, R_S and R_Q, thus enabling Monte Carlo and parametric simulations over the whole SiPM. In spite of longer computation time, with this second approach it is possible to investigate either SiPM response uniformity, when the incoming single photon is focused on different positions over the active area, or the overall current build-up, when few or many photons hit in different x-y positions and at different times.

IV. MODEL VALIDATION

We validated the microcell model and the two simulation approaches. At first, we simulated and compared the two models in the same conditions (SiPM parameters, electronics and photon excitation). Then, the simulated transient waveform was compared to the expected analytical trend. Finally, we used the *two macrocells approach* to simulate different operating conditions and results were compared to experimental measurements on both vertical and horizontal current-flow SiPMs.

A. Comparison of the Two Approaches

We compared the two proposed approaches by means of SPICE simulations in the same conditions, which are same microcells' model parameters, same number of total and fired microcells, no parasitic interconnects resistors in the *array approach*. In detail, we simulated a 16×16 array with 1 firing microcells and typical SiPM values ($V_{BD} = 25$ V, $V_{EX} = 5$ V, $R_D = 400$ Ω, $C_D = 50$ fF, $R_Q = 200$ kΩ, $C_Q = 1$ fF, $C_G = 6$ fF each), reading out the avalanche current signal on a 50 Ω sensing resistor placed in series to the SiPM. The two approaches perfectly match, as shown in Fig. 5(a). Fig. 5(b) shows the first portion of the output waveforms when the avalanche is ignited in different microcells, by using the *array* model with 2 Ω stray resistances between adjacent microcells. This value is overestimated for adjacent microcells, but it is useful to understand the behavior of SiPMs with thousands
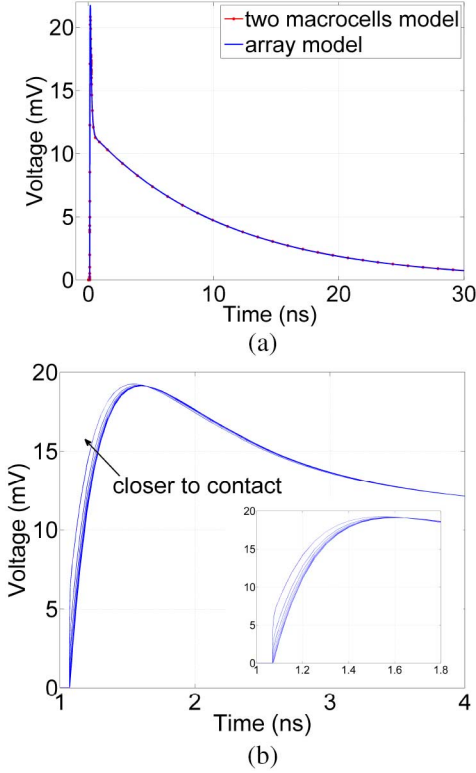
Fig. 5. Perfect matching of the two simulation approaches, in the same conditions (SiPM parameters, electronics and photon excitation) (a), and differences between microcells in the array model (b), in the first few ns of the peak (see also the inset with a zoom in).

of microcells. Microcells closer to anode or cathode contacts show faster (and slightly higher) response compared to those in the array center. Clearly, the *two macrocells* approach cannot highlight such differences.

The *array* model is the most accurate, but also more computational demanding, hence with longer simulation time: for example the simulations in Fig. 5(a) require a computation time of 0.02 s and 6.5 s, respectively.

B. Comparison of Simulations vs. Analytical Analysis

We analytically studied the SiPM behavior, by considering a single fired microcell out of 400 total microcells, omitting the quenching resistance of quiescent microcells. In order to linearize the circuit, for the analytical study we applied an input step voltage generator with amplitude equal to the excess bias V_{EX}. The resulting circuit is shown in Fig. 6(a): R_L is the 50 Ω external load resistance of the oscilloscope, C_{eq} represents all quiescent microcells and grid capacitance (C_G) and it is given by:

$$C_{eq} = (N-1) \cdot \frac{C_Q C_D}{C_Q + C_D} + N \cdot C_G \qquad (1)$$

We computed the waveform of the current through the load, confirming what already reported in [16]:

$$i_L(t) = I_f \cdot \left(1 - \frac{\tau_q - \tau_i}{\tau_d - \tau_i} \cdot e^{-\frac{t}{\tau_i}} + \frac{\tau_q - \tau_d}{\tau_d - \tau_i} \cdot e^{-\frac{t}{\tau_d}}\right) \qquad (2)$$
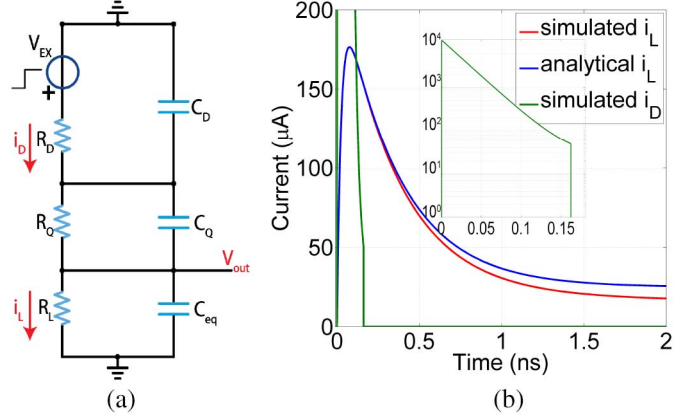

Fig. 6. (a) Simplified SiPM schematics for analytical analysis. Note that C_{eq} takes into account all not-firing microcells. (b) Simulated (red) and analytical (blue) external load current i_L and simulated internal avalanche current i_D (green), cropped and, in the inset, uncropped in logarithmic scale.

I_f is the asymptotic current level, τ_q is the time constant of the zero introduced by C_Q, instead τ_i and τ_d are the two poles' fast and slow (dominant) time constants, respectively, given by:

$$I_f = \frac{V_{EX}}{R_D + R_Q + R_L}$$
$$\tau_q = C_q R_q$$
$$\tau_i \approx \frac{R_d (C_d + C_q) \cdot R_L C_{eq}}{R_d (C_d + C_q) + R_L C_{eq}}$$
$$\tau_d \approx R_d (C_d + C_q) + R_L C_{eq} \qquad (3)$$

The peak current can be computed by nulling the first derivative of Eq. (2), thus obtaining:

$$i_L^{peak} = I_f \cdot \left\{1 + \frac{\tau_q - \tau_d}{\tau_d} \cdot \left[\frac{\tau_i}{\tau_d} \cdot \frac{(\tau_q - \tau_d)}{(\tau_q - \tau_i)}\right]^{\frac{\tau_i}{\tau_d - \tau_i}}\right\} \qquad (4)$$

Fig. 6(b) shows simulated (red) and analytical (blue) current waveforms through the load resistor and the simulated avalanche current flowing internally through the detector resistor (green), with realistic values of $V_{EX} = 5$ V, $R_D = 400 \, \Omega$, $R_Q = 200 \, k\Omega$, $R_L = 50 \, \Omega$, $C_D = 50 \, fF$, $C_Q = 15 \, fF$, $C_{eq} = 7 \, pF$. The inset shows the entire i_D waveform, which is two orders of magnitude higher than the load current, since most of the avalanche current charges the parasitic capacitances and does not reach the load resistor, hence cannot be measured [22]. For this reason, when designing a SiPM, it is very important to minimize the stray C_D and to trade-off the R_Q value, being high enough for proper quenching, but sufficiently low to assure a fast recovery and to provide a measurable output current pulse, even in case of low C_Q value.

Note that the proposed SPICE model is able to simulate the avalanche self-quenching and in fact the internal avalanche current instantaneously drops to zero when it decreases below the 50 μA threshold [22], thanks to switch SW2 that, instead, is not included in the analytical analysis. This is the reason why in Fig. 6(b) simulated and analytical load currents perfectly match

Parameter	Computed from simulation	Analytical analysis	Units
τ_i	25.1	25.9	ps
τ_d	376.1	350.7	ps
i_L^{peak}	176.5	176.6	μA

before self-quenching, then they separate because the analytical curve reaches its asymptotic value I_f, whereas the simulated one quenches to zero (with a slow time constant $\tau_s \approx (C_D + C_Q) \cdot R_Q = 13$ ns). The values of the load current waveform shown in Fig. 6(b) (i.e. fast-rising edge time constant τ_i, slow-falling decay time constant τ_d, peak load current i_L^{peak}) are in agreement with the analytical Eqs. (1), (2) and (3), as proved in Table I.

We extracted the time constants from simulation plots through the following equations:

$$\tau_i = \frac{t_2 - t_1}{\ln\left(y_1 - i_d^{peak}\right) - \ln\left(y_2 - i_d^{peak}\right)}$$

$$\tau_d = \frac{t_4 - t_3}{\ln(y_3) - \ln(y_4)} \tag{5}$$

in which t_1, t_2, t_3, t_4 and y_1, y_2, y_3, y_4 are four generic points of the waveform, two (#1-2) along the rising edge and two (#3-4) along the falling decay.

C. Comparison of Simulations vs. Measurements

In order to compare simulations with real measurements, we employed the transimpedance configuration shown in Fig. 7, and not just a single 50 Ω sensing resistor, because it would lead to poor Signal-to-Noise Ratio (SNR). The amplifier model was also added in the simulation. We tested a vertical current-flow SiPM (Excelitas c30742-11, 20×20 microcells [23]) and a horizontal current-flow SiPM (PoliMI [12]) by means of a current feedback amplifier (Texas Instruments LMH6702). We measured SiPM parameters by means of a curve tracer (Tektronics 370) and a network analyzer (HP 8753d), following the procedure described in [24]. Vertical current-flow SiPM values are consistent with the parameters provided by the manufacturer ($V_{BD} = 100$ V, $R_Q = 1.2$ MΩ, $R_D = 400$ Ω, $C_D = 50$ fF, $C_Q = 18$ fF, $C_G = 6$ fF for each microcell); horizontal current-flow SiPM values match those extracted through Virtuoso RCX during design ($V_{BD} = 25$ V, $R_Q = 164$ kΩ, $R_D = 300$ Ω, $C_D = 180$ fF, $C_Q = 2.5$ fF, $C_{AS} = 0.1$ fF, $C_{CS} = 45$ fF, $C_G = 5$ fF for each microcell).

We tested the capability of the model to correctly simulate SiPMs in two real cases by keeping the SiPM in dark and having just one firing microcell (a dark count) and two different simultaneously firing microcells (a dark count and a cross-talk ignition). Fig. 8 and Fig. 9 show the good matching between simulations and measurements for the vertical and the horizontal current-flow SiPMs. Measurements were acquired with the oscilloscope in persistence mode (and were also inverted for sake of
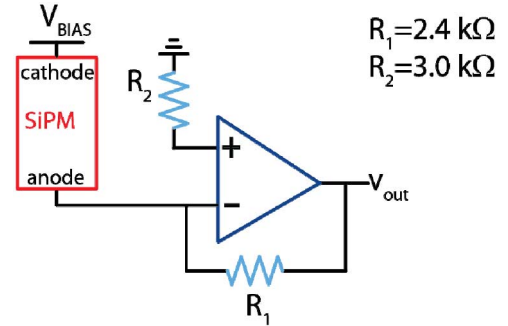

Fig. 7. Transimpedance configuration used to validate simulations.
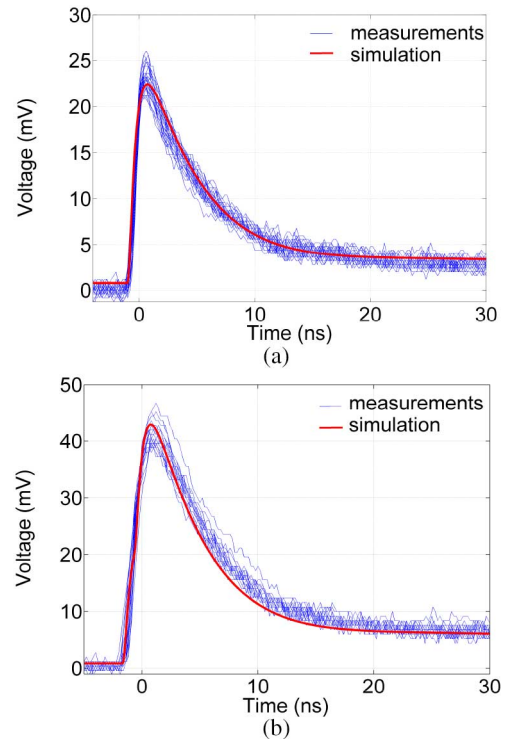
$R_1 = 2.4$ kΩ
$R_2 = 3.0$ kΩ

Fig. 8. Vertical current-flow SiPM: simulation (red curve) vs. measurements (blue traces) for (a) one firing microcell and (b) two microcells simultaneously firing (i.e. overlapping current pulses).

clarity). We found the same agreement also with higher number of firing microcells, as long as the transimedance amplifier is not brought too close to saturation. The reason why here we report just one or two photon excitation is to highlight the spread in the measured traces, due to the different position and mismatches among the randomly fired microcells, without suffering by excessive broadening of many-photon absorption (see the following Fig. 12). Moreover, in Fig. 8 the final amplitude looks not zero, because the entire discharge transient is dominated by the slow time constant $\tau_s \approx (C_D + C_Q) \cdot R_Q = 81.6$ ns (or 85.1 ns when computed from measurements and Eq. (5)). Instead the fast time constant before quenching (τ_i and τ_d) are not visible because smoothed by the 30 MHz transimpedance amplifier bandwidth (as simulated and confirmed by experimental measurements). In Fig. 9 the decay is faster, since $\tau_s \approx$
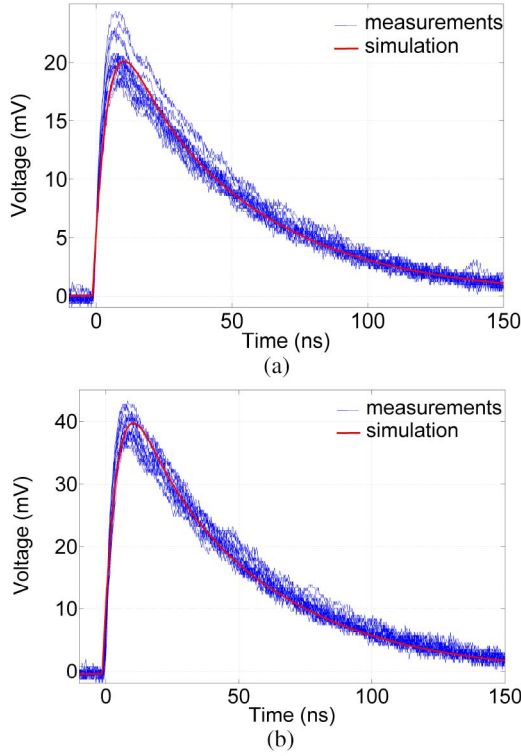
Fig. 9. Horizontal current-flow SiPM: simulation (red curve) *vs.* measurements (blue traces)for (a) one firing microcell and (b) two microcells simultaneously firing (i.e. overlapping current pulses).
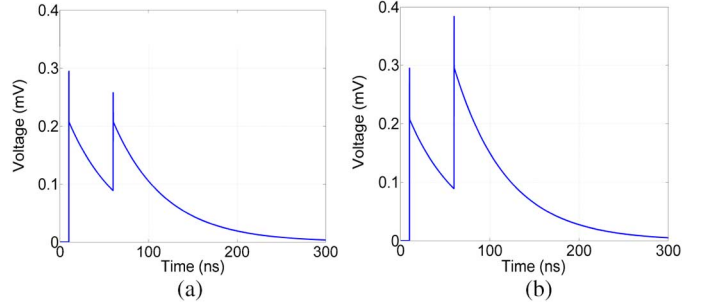

Fig. 10. Simulation of two avalanches with 50 ns time separation, hitting (a) the same microcell and (b) two different microcells.

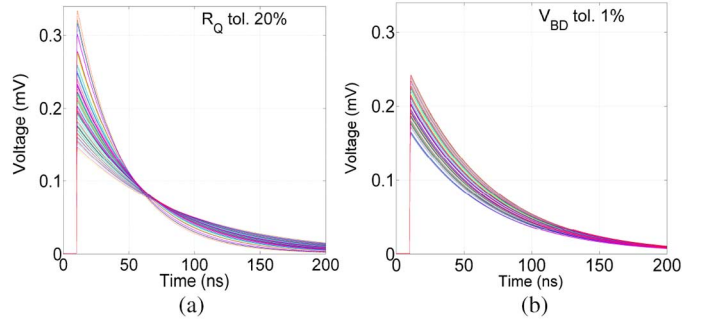Fig. 11. A set of 100 Monte Carlo simulations with (a) 10% variation on R_Q and (b) 1% spread of V_{BD}.

$(C_D + C_Q + C_A) \cdot R_Q = 29.6$ ns (or 32.3 ns from measurement and Eq. (5)).

V. DETAILED SIMULATIONS

Many simulations were performed in order to investigate SiPM behaviors in different operating conditions. The simulated transient waveforms represent the voltage across a 50 Ω sensing resistor connected in series to the SiPM, when using 5 V excess bias. In particular we report on pile-up effects, statistical spreads due to processing mismatches, photoelectron spectrum, and differences in transient responses when varying N and F, eventually we provide some design criteria.

A. Pile-up Effects

We studied the SiPM response when two avalanches are triggered separated by 50 ns either within the same microcell or into two different microcells. We employed the *array approach* and simulated an 8×8 vertical current-flow SiPM (microcells with $R_D = 400$ Ω, $C_D = 50$ fF, $R_Q = 1.2$ MΩ, $C_Q = 0.05$ fF, $C_G = 6$ fF), with no stray resistances between microcells. As shown in Fig. 10, the fast peak is due to the quenching C_Q capacitance while the slower time constant is due to the quenching resistance R_Q [25]. According to analytical analysis, the fast rising time constant (almost vertical, from 0 to 300 μV) is given by $\tau_i = 9.8$ ps (or 9.1 ps as extracted from simulation), the first fast decay time constant (almost vertical, from 300 μV to 200 μV) is $\tau_d = 40.2$ ps (38.8 ps from simulation), the second slow decay time constant (after avalanche quenching, i.e. from 200 μV down to 0) is $\tau_s = 61$ ns (65 ns from simulation). When avalanches are ignited in the same microcell, the second

fast peak is lower than the first one (see Fig. 10(a)), because the SPAD has not yet recovered the quiescent bias (i.e. the actual excess bias is lower than the nominal V_{EX} one); instead the second slow decay starts at the same amplitude, because only that microcell is fired, hence current is V_{EX}/R_Q. When avalanches are ignited in different microcells, the current contributions sum-up independently (see Fig. 10(b)), thus resulting in a "risen" second pulse (both fast peak and slow decay attack), since it lays over the tail of the first one.

It is worth noting that, in photon timing application, the pile-up in different microcells (e.g. when light is not focused into a single microcell) causes time-jitter, because the output voltage crosses the comparator threshold at different time delays. For this reason, applications that measure the time stamp of each photon with a fixed threshold are affected by such a pile-up effect [26]. This suggests to introduce high-pass filtering in SiPM front-ends in order to reduce the duration of each output pulse, hence the potential superposition of two or more pulses, and thus also pile-up probability.

B. Statistical Spreads and Tolerances

We analyzed the effects of statistical spreads of R_Q (20% tolerance) and V_{BD} (1% tolerance) through the 8×8 *array approach* of a vertical current-flow SiPM with no C_Q, due to possible processing non-uniformities. Fig. 11 shows the results from 100 Monte Carlo simulations: R_Q tolerance impacts both peak amplitude (20% variation) and slow time constant (17% variation), whereas V_{BD} tolerance impacts just peak voltage (16% variations), as expected from Eqs. (3) and (4). We chose 20% tolerance of R_Q, definitely overestimated for small SiPMs, but somehow reasonable for large (thousands of microcells)
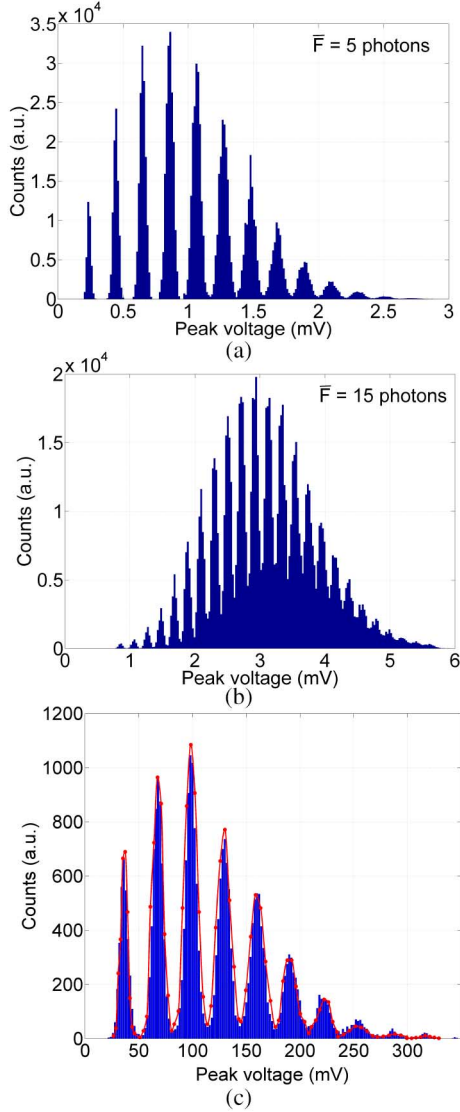
Fig. 12. Simulated photoelectron spectrum at different illumination conditions, namely (a) 5 photons and (b) 15 photons on average, and (c) comparison between simulated (blue) and measured (red) photoelectron spectrum (4 photons on average) of a 1 mm × 1 mm Excelitas SiPM.

SiPMs, for showing that the voltage peak almost doubles over the spread extremes, thus possibly causing a misleading readout of 2 photons instead of 1 single photon.

C. Photoelectron Spectrum

The photoelectron spectrum is an important parameter in SiPMs performance characterization, because it enlightens the capability to resolve a number of simultaneous photons hitting the detector. The probability to detect F (firing) simultaneous photons is described by a Poisson distribution:

$$P(F) = e^{-\bar{F}} \cdot \frac{\bar{F}^F}{F!} \qquad (6)$$

where $\bar{F}$ is the mean value of the distribution.

We simulated two distributions, with mean values $\bar{F}$ of 5 and 15 photons and 10^6 total number of events. We computed through Matlab the probability distribution function P(F), with
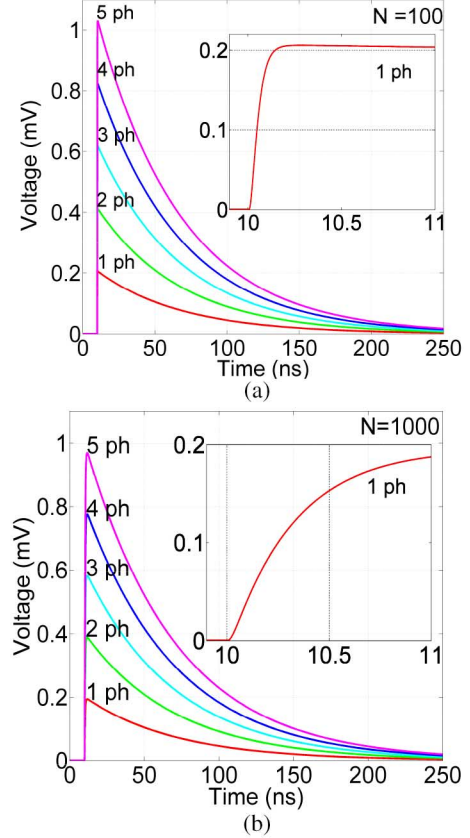

Fig. 13. Simulation transients for (a) 100 and (b) 1000 microcells SiPMs, when considering from 1 to 5 simultaneously firing microcells. The insets show a zoom-in of the 1-photon rising edge.

F varying from 1 to 15 when $\bar{F} = 5$ and from 1 to 30 when $\bar{F} = 15$. Then we performed SPICE Monte Carlo simulations with the 8×8 *array approach*, with 0.2% tolerance on V_{BD} and 5% on R_Q. Fig. 12(a) and (b) shows the avalanche amplitude distribution of each simulation, weighted for the probability to have F photons. As it can be seen, the mean value of the peak voltage amplitude increases linearly with the number of firing microcells, and its standard deviation increases with the square root of the firing microcells, as expected from theory. Fig. 12(c) compares simulated and measured photoelectron spectrum for a 1 mm × 1 mm Excelitas SiPM coupled to a transimpedance amplifier, when the photon flux was about 4 photons on average: the matching is excellent when considering 2% tolerance on R and 0.5% on V_{BD} during SPICE simulations.

D. SiPM Response when Varying N and F

We analyzed the SiPM transient response with different numbers of total microcells (N) and firing microcells (F). At first, we considered two SiPMs (N = 100 and N = 1000) and we varied the number of firing microcells F from 1 to 5. Fig. 13 shows the responses simulated with the *two macrocells* approach. For both SiPMs, the peak amplitude increases linearly with the number of firing cells; however for the 1000 microcells SiPM the peak is lower and rising edge is slower (as shown in the inset of Fig. 13, just for the 1 photon waveform). Such an effect, due to a large number of microcells (hence to a large grid capacitance), is similar to a low pass filtering of the output pulse.
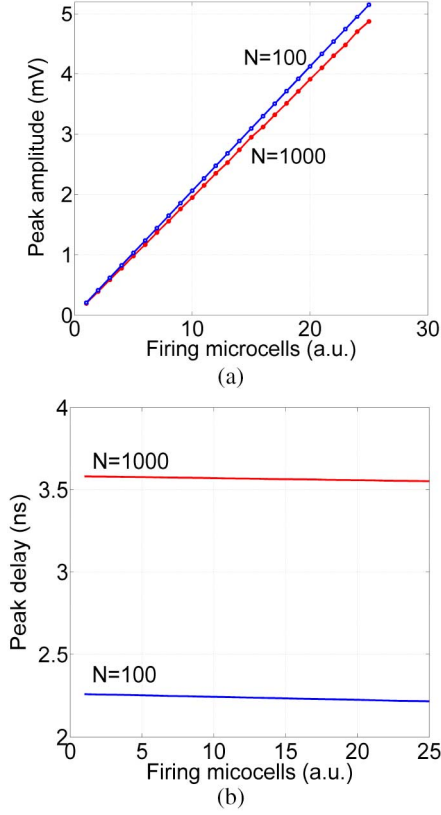
Fig. 14. (a) Peak amplitude and (b) peak delay *vs.* number of firing microcells, in a N = 100 and a N = 1000 microcells SiPM.
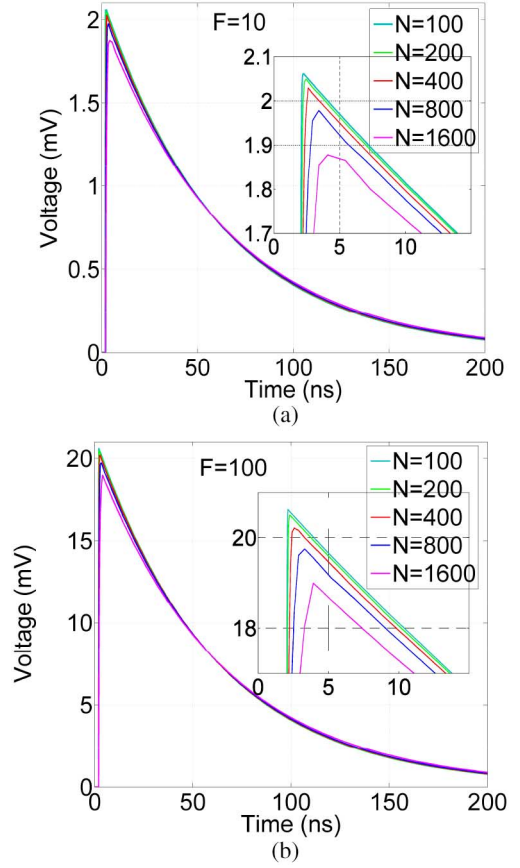

Fig. 15. Simulated waveforms with (a) 10 and (b) 100 firing microcells, for SiPMs with a total number of microcells equal to 100, 200, 400, 800, 1600.

It is interesting to plot the relationship between peak amplitude and peak delay *vs.* the number of firing cells. Fig. 14 shows these trends for the two SiPMs (100 and 1000 microcells each): the peak amplitude grows linearly with the number of firing cells F; and the larger the SiPM, the slower its response, i.e. the more delayed the peaks gets. Moreover, the response becomes slightly faster (lower peak delay) when increasing F.

In a second set of simulations, we considered a constant number of firing microcells (F = 10 or 100), whereas the SiPM size was increased (N = 100, 200, 400, 800, 1600). Fig. 15 shows the SiPM transient response, while Fig. 16 shows peak amplitude and peak delay *vs*. total number of microcells. What observed in Fig. 13 and Fig. 14 is confirmed also here: larger SiPM provides more delayed signal peak, whereas more coincident photons (i.e. firing microcells) result in higher and faster peak.

Similar results were obtained in [16] through an analytical analysis, whereas we did not observe the non-proportionality of SiPM signal with the number of firing microcells, as shown in [18], because in our simulation we considered few simultaneous photons.

E. Horizontal vs. Vertical Current-flow SiPMs

As shown in Fig. 1, SiPM can have just two contacts or even a third (substrate) one, depending on the fabrication technology and the main direction (either vertical or horizontal) of the avalanche current flow.

We compared the transient waveforms of horizontal current-flow SiPMs when connecting the sensing resistor (50 Ω) or the transimpedance amplifier either to the cathode or to the anode. Whereas in vertical current-flow SiPMs (being dipoles) the two sensing schemes are identical, in horizontal current-flow SiPMs the presence of the substrate contact introduces a strong asymmetry, as shown in Fig. 17(a), since C_{AS} and C_{CS} have very different values and usually $C_{CS} \gg C_{AS}$ (C_{AS} almost null, C_{CS} about 100 fF). In particular, when R_S is connected to the cathode, the waveform is lower peaked and slower, due to the low-pass filtering action of C_{CS}.

Fig. 17(b) shows the output waveform when the SiPM signal is read by means of a transimpedance amplifier (2.4 kΩ R_F feedback resistance) sensing either the cathode or the anode, respectively. With such a readout, C_{CS} has no influence in both cases because it is either connected to constant bias (anode readout) or to virtual ground (cathode readout). The two waveforms differ because with anode readout only the current through $R_Q//C_Q$ flows into R_F, whereas with cathode readout the current through $R_Q//C_Q$ adds to the C_{AS} contribution to the output voltage. As shown in Fig. 17(b), simulated results and experimental measurements match very well. The different output waveforms, due to the different readout, must be properly taken into account when designing a SiPM device or the corresponding readout circuitry, due to the strong impact on the achievable timing resolution.
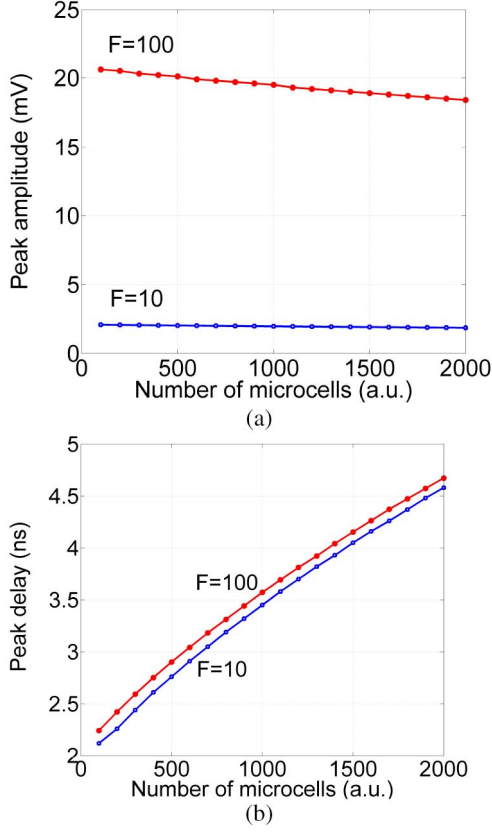
Fig. 16. (a) Peak amplitude and (b) peak delay *vs*. SiPM size (i.e. total number N of microcells), with F = 10 and F = 100 firing microcells.
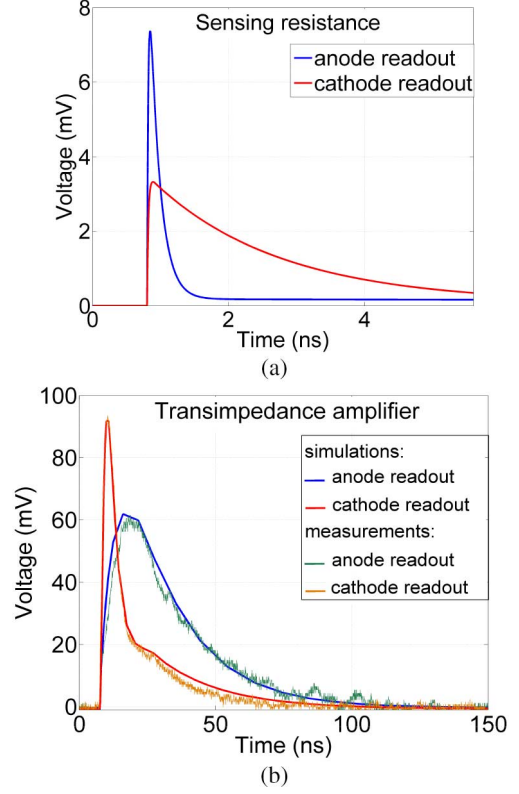

Fig. 17. Comparison between cathode and anode readout in a horizontal current-flow SiPM, with a 50 Ω sensing resistance (a) and with a transimpedance amplifier (b). The latter are compared to experimental data and the matching is excellent. In both cases the substrate was grounded.
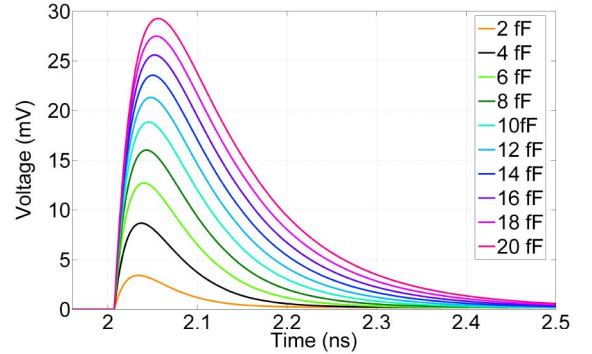
Eventually, when comparing Fig. 17(a) and (b), we observe that the 50 Ω sensing resistance readout provides a faster avalanche signal since it is not limited by the transimpedance amplifier's bandwidth, but with smaller amplitude.

VI. SiPM Design Criteria

The proposed model can be exploited to correctly choose the passive components parameters (R_Q and C_Q in particular) during the SiPM design phase. The model helps when studying the dependence of SiPM transient response on the values of C_Q and R_Q and on the microcells mismatch.

Fig. 18 shows the response of a single microcell with different C_Q, from 2 fF to 20 fF: such capacitor, by shunting the quenching resistor, provides a steeper slope of the avalanche build-up and a higher peak amplitude. Therefore, adding a capacitance in that position is very useful especially in photon timing applications [27], [28].

The effect of different values of R_Q (from 90 kΩ to 1 MΩ) is shown in Fig. 19. If R_Q has too low a value, the microcell cannot self-quench (see the highest curve in Fig. 19, corresponding to $R_Q = 90$ kΩ), but keeping R_Q as low as possible has the advantage of increasing the available current for external readout and of providing faster recovery time [29]. Note that in Fig. 19 all voltage waveforms must have same area (apart from the plots corresponding to $R_Q = 90$ kΩ when the avalanche is not quenched), because it is equal to the charge accumulated within

Fig. 18. Microcell transient response with different values of C_Q.

the parasitic capacitances (usually normalized to the electron charge and called "gain"), given by:

$$Q = C_{tot} \cdot V_{EX} \qquad (7)$$

where C_{tot} is total capacitance from cathode to anode, and hence the higher the peak amplitude, the shorter the decay.

From Fig. 19 we observe that the lower the R_Q, the higher the peak amplitude and the fastest the slow tail. Hence, when designing the SiPM the best solution is to choose an R_Q high enough to quench the avalanche, but sufficiently low to provide fast and peaked response.

Finally, we studied the effects of mismatches among microcells, which can be deterministic (e.g. due to interconnects para-
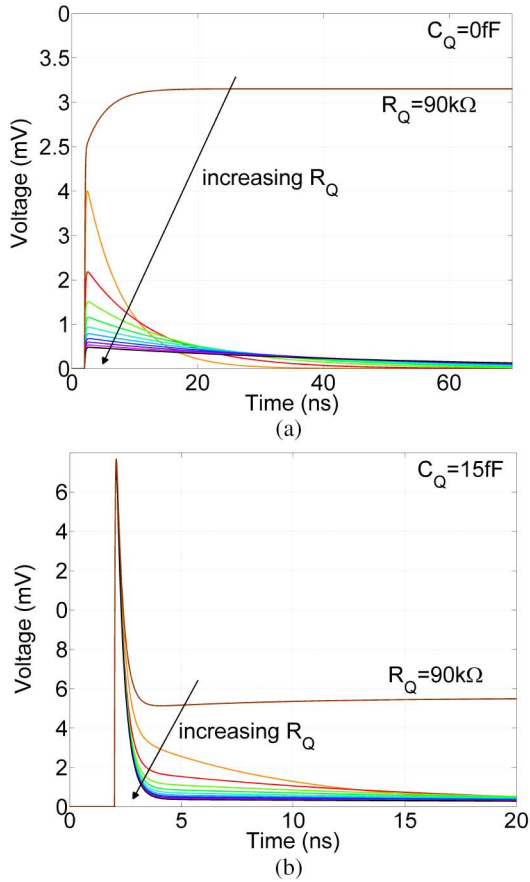
Fig. 19. Microcell transient response when varying the value of R_Q, (a) with no quenching capacitor and (b) with $C_Q = 15$ fF.

Fig. 20. Transient responses when a microcell close to or far away from the contacts gets triggered, in an 8×8 (a) and 20×20 (b) SiPM.

Fig. 21. Detection time distribution of 1000 Monte Carlo simulations with just one fired microcell, due to 1% V_{BD} and 20% R_Q tolerances.

sitic resistances between different microcells) or statistical (e.g. parameters spreading). In particular, we studied timing jitter between microcells close to external contacts and those far away (e.g. at the center of the SiPM). We employed the *array approach* for 8×8 and 20×20 SiPMs and included a $7\,\Omega$ stray resistance between adjacent microcells (see Fig. 4(b)). Fig. 20 shows the SiPM responses when the fired microcell is close to or away from the contacts. By setting a threshold at 1/3 of the peak value, the time delay is 2 ps (8×8 array) and 10 ps (20×20 array).

We computed the timing jitter by means of 1000 Monte Carlo simulations, in which we measured the threshold crossing timing when just one microcell was fired (with no stray resistance). Fig. 21 shows the detection time distribution, with a timing jitter of 12.6 ps FWHM (Full-Width at Half Maximum) when considering 1% variations on V_{BD} and 20% tolerance on R_Q. By comparing Fig. 20 with Fig. 21, it is possible to observe that small SiPM (e.g. 8×8) with $7\,\Omega$ stray resistances shows a completely negligible deterministic contribution when compared to the jitter introduced by statistical processing spreads. Instead, by increasing the SiPM size (e.g. 20×20) the two contributions become comparable.

VII. Conclusions

We presented and thoroughly discussed two approaches for electrical simulations of SiPM detectors, based on a same SPICE electrical model for the microcell. The models
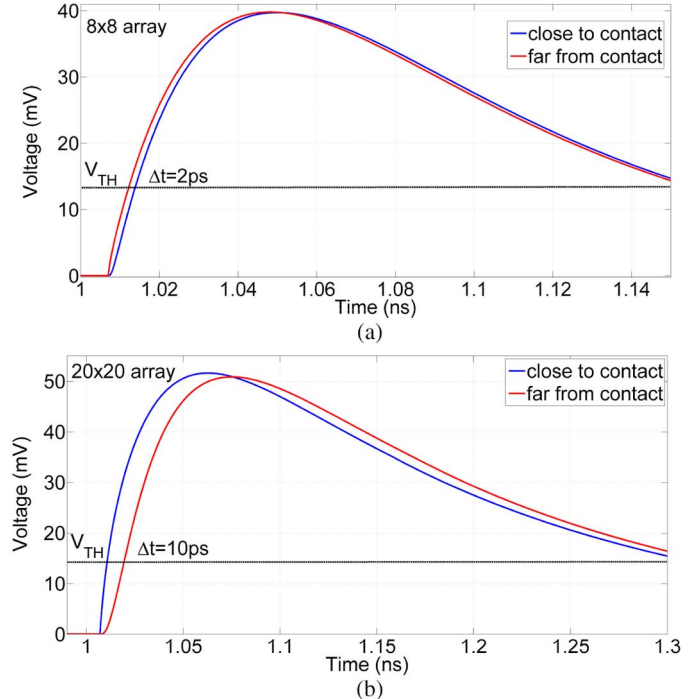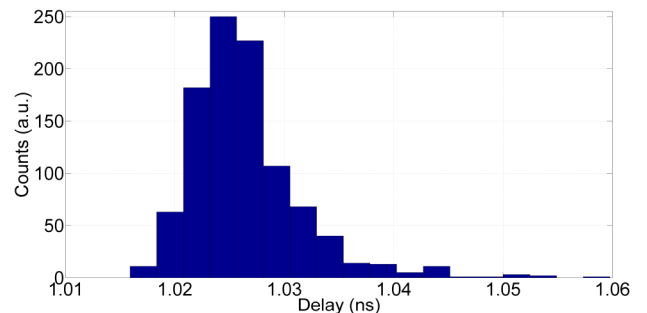
accurately predict the avalanche current build-up and its self-quenching, and properly take into account all parasitic effects and parameter spreads. To the best of our knowledge, for the first time in literature, a SPICE model is able to simulate also CMOS SiPMs with substrate contact. Our model can be augmented by adding statistical behaviors, such as dark counts, afterpulsing, and crosstalk, as done in [30] for SPADs.

The models can be used either for choosing the best readout electronic circuit for a given commercially-available SiPM or for accurately designing a brand new SiPM, given the optical and readout specifications and constraints.

We presented many simulations using two approaches and with different model parameters. The *two macrocells* approach is preferred to study large SiPMs, limiting the observations to simultaneous photon ignitions. In particular, this model was used to analyze SiPM transient responses (amplitude and delay) when varying the total number N and the firing number F of microcells. Instead, the *array approach* allows to get a much better insight on time-separated ignitions and also on

mismatches between microcells. In particular this model was used to study the avalanche pulses pile-up effect, to analyze deterministic and statistical mismatches inside different SiPMs, and to extract the SiPM photoelectron spectrum.

REFERENCES

[1] F. Zappa, S. Tisa, A. Tosi, and S. Cova, "Principles and features of single-photon avalanche diode arrays," *Sens. Actuators A Phys.*, vol. 140, pp. 103–112, 2007.

[2] A. Osovizky, I. Cohenzada, V. Pushkarsky, D. Ginzburg, E. Vulaski, and M. Ellenbogen, "Silicon photomultiplier technology review and experimental results," in *Proc. Conf. Nuclear Societies in Israel*, 2008, vol. 40, no. 05.

[3] T. Frach, G. Prescher, C. Degenhardt, R. de Gruyter, A. Schmitz, and R. Ballizany, "The digital silicon photomultiplier - principle of operation and intrinsic detector performance," in *Proc. IEEE Nuclear Science Symp.*, 2009.

[4] P. Berard, M. Couture, P. Deschamps, F. Laforce, and H. Dautet, "Performance measurement for a new low dark count UV-SiPM," in *Proc. IEEE Nuclear Science Symp. and Medical Imaging Conf.*, Oct. 2011, pp. 544–547, doi: 10.1109/NSSMIC.2011.6154109.

[5] P. Bérard, M. Couture, F. Laforce, B. Fong, and H. Dautet, "Characterization of an SiPM dedicated at analytical, life science, and medical imaging," *Proc. SPIE, Optical Components and Materials X*, vol. 8621, Mar. 2013, doi: 10.1117/12.2001520.

[6] K. Yamamoto, K. Yamamura, K. Sato, T. Ota, H. Suzuki, and S. Ohsuka, "Development of multi-pixel photon counter (MPPC)," in *Proc. IEEE Nuclear Science Symp. Conf. Rec.*, Oct.–Nov. 2006, vol. 2, pp. 1094–1097, doi: 10.1109/NSSMIC.2006.356038.

[7] T. Nagano, K. Sato, A. Ishida, T. Baba, R. Tsuchiya, and K. Yamamoto, "Timing resolution improvement of MPPC for TOF-PET imaging," in *Proc. IEEE Nuclear Science Symp. and Medical Imaging Conf.*, Oct.–Nov. 2012, pp. 1577–1580, doi: 10.1109/NSSMIC.2012.6551376.

[8] J. D. Thiessen, C. Jackson, K. O'Neill, D. Bishop, P. Kozlowski, and F. Retiere *et al.*, "Performance evaluation of sensl SiPM arrays for high-resolution PET," in *Proc. IEEE Nuclear Science Symp. and Medical Imaging Conf.*, Oct.–Nov. 2013, pp. 1–4, doi: 10.1109/NSSMIC.2013.6829318.

[9] C. Jackson, K. O'Neill, L. Wall, and B. McGarvey, "High-volume silicon photomultiplier production, performance, and reliability," *Proc. SPIE Opt. Eng.*, vol. 53, no. 8, 2014, doi: 10.1117/1.OE.53.8.081909.

[10] C. Jackson, L. Wall, K. O'Neill, B. McGarvey, and D. Herbert, "Ultra-low noise and exceptional uniformity of sensl C-series SiPM sensors," *Proc. SPIE Opt. Eng.*, vol. 53, no. 8, 2014.

[11] C. Dietzinger, T. Ganka, A. Márquez Seco, N. Miyakawa, P. Iskra, and F. Wiest, "Improved SiPM device performance by introduction of a new manufacturing technology," *Proc. SPIE, Photonic Fiber and Crystal Devices: Advances in Materials and Innovations in Device Applications VII*, vol. 884703, Sep. 2013, doi: 10.1117/12.2027101.

[12] F. Villa, D. Bronzi, M. Vergani, Y. Zou, A. Ruggeri, F. Zappa, and A. Dalla Mora, "Analog SiPM in planar CMOS technology," in *Proc. Eur. Solid-State Device Research Conf.*, 2014, pp. 294–297.

[13] Documentation [Online]. Available: http://www.cadence.com/products/pcb/spice/

[14] A. K. Jha, H. T. van Dam, M. A. Kupinski, and E. Clarkson, "Simulating silicon photomultiplier response to scintillation light," *IEEE Trans. Nucl. Sci.*, vol. 60, no. 1, pp. 336–351, Feb. 2013.

[15] F. Ciciriello, F. Corsi, F. Liciulli, C. Marzocca, and G. Matarrese *et al.*, "Accurate modeling of SiPM detectors coupled to FE electronics for timing performance analysis," *Nucl. Instrum. Methods Phys. Res. A*, vol. 718, pp. 331–333, 2013.

[16] D. Marano, M. Belluso, S. Bonanno, S. Billotta, A. Grillo, and S. Garozzo *et al.*, "Silicon photomultipliers electrical model extensive analytical analysis," *IEEE Trans. Nucl. Sci.*, vol. 61, no. 1, pp. 23–34, Feb. 2014.

[17] D. Marano, G. Bonanno, M. Belluso, S. Billotta, and A. Grillo *et al.*, "Improved SPICE electrical model of silicon photomultipliers," *Nucl. Instrum. Methods Phys. Res. A*, vol. 726, pp. 1–7, 2013.

[18] S. Seifert, H. T. van Dam, J. Huizenga, R. Vinke, P. Dendooven, H. Lohner, and D. R. Schaart, "Simulation of silicon photomultiplier signals," *IEEE Trans. Nucl. Sci.*, vol. 56, no. 6, pp. 3726–3733, Dec. 2009.

[19] G. Condorelli, D. Sanfilippo, G. Valvo, M. Mazzillo, and D. Bongiovanni *et al.*, "Extensive electrical model of large area silicon photomultipliers," *Nucl. Instrum. Methods Phys. Res. A*, vol. 654, pp. 126–134, 2011.

[20] F. Zappa, A. Tosi, A. Dalla Mora, and S. Tisa, "SPICE modeling of single photon avalanche diodes," *Sens. Actuators A Phys.*, vol. 153, no. 2, pp. 197–204, 2009.

[21] G. Cho, H. Kim, W. Suk Sul, C. Lee, and B. Kang, "Optimum design of quenching capacitor integrated silicon photomultipliers for TOF-PET application," *Phys. Procedia*, vol. 37, pp. 1511–1517, 2012.

[22] S. Cova, M. Ghioni, A. Lacaita, C. Samori, and F. Zappa, "Avalanche photodiodes and quenching circuits for single-photon detection," *Appl. Opt.*, vol. 35, no. 12, pp. 1956–1976, 1996.

[23] Excelitas datasheet [Online]. Available: www.excelitas.com/Downloads/DTS_C30742-11-050_Series_SiPM.pdf

[24] E. Popova, B. Dolgoshein, P. Buzhan, A. Ilyin, and A. Stifutkin *et al.*, "Evaluation of high UV sensitive SiPMs from MEPhI/MPI for use in liquid argon," in *Proc. Science, Int. Workshop New Photon-Detectors*, 2012.

[25] K. A. Wangerin, G. Wang, C. Kim, and V. Danon, "Passive electrical model of silicon photomultipliers," in *Proc. IEEE Nuclear Science Symp. Conf. Rec.*, 2008.

[26] A. Gola, C. Piemonte, and A. Tarolli, "Analog circuit for timing measurements with large area sipms coupled to lyso crystals," *IEEE Trans. Nucl. Sci.*, vol. 60, no. 2, pp. 1296–1302, Apr. 2013.

[27] F. Acerbi, M. Cazzanelli, A. Ferri, A. Gola, L. Pavesi, N. Zorzi, and C. Piemonte, "High detection efficiency and time resolution integrated-passive-quenched single-photon avalanche diodes," *IEEE J. Sel. Topics Quantum Electron.*, vol. 20, no. 6, pp. 268–275, Nov.–Dec. 2014.

[28] C. Lee, W. S. Sul, H. Kim, C. Kim, and G. Cho, "Effect on MIM structured parallel quenching capacitor of SiPMs," *Nucl. Instrum. Methods Phys. Res. A*, vol. 650, no. 1, pp. 125–128, 2011.

[29] T. Nagano, K. Sato, A. Ishida, T. Baba, R. Tsuchiya, and K. Yamamoto, "Timing resolution improvement of MPPC for TOF-PET imaging," in *Proc. IEEE Nuclear Science Symp. and Medical Imaging Conf.*, 2012, pp. 1577–1580, doi: 10.1109/NSSMIC.2012.6551376.

[30] G. Giustolisi, R. Mita, and G. Palumbo, "Behavioral modeling of statistical phenomena of single-photon avalanche diodes," *Int. J. Circ. Theor. Appl.*, vol. 40, no. 7, pp. 661–679, 2012.